A Modified Mroz Model for Springback Prediction

Danielle Zeng and Z. Cedric Xia

A new anisotropic material hardening model is introduced in this study for springback simulation. It is modified from the Mroz multi-yield surface hardening model and incorporated more realistic Bauschinger effect for cyclic loading and anisotropic yield surfaces for sheet metals. The model is targeted for sheet metal forming simulations where the accurate springback predictions are important, and where materials have more rapid hardening characteristics and ability to sustain higher stresses such as so-called advanced high-strength steels (AHSS). The constitutive integration algorithm is derived and it is numerically implemented in the commercial FEA code via a user-material subroutine. The new model is applied to a U-channel forming test with DP600 steel. Experiments are conducted and springback results are compared with numerical prediction to demonstrate the new model's effectiveness.

1. Introduction

Springback is an important issue for part and die design in the manufacturing of automotive sheet metal components. Elimination or correction of springback has to be made during the design stages to obtain a final part shape matching its design intent. Otherwise it will produce dimensional deviations and result in assembly difficulties. Traditionally, die engineers put a great effort to either reduce or compensate for springback based on trial-and-error. Numerous die re-cuts are often needed in order to obtain a dimensionally accurate part. This approach is not only time consuming but also costly.

Due to weight reduction efforts to meet fuel economy pressure and increase vehicle safety requirement, the use of advanced high-strength steel (AHSS) sheets such as dual-phase (DP) and transformation induced plasticity (TRIP) alloys has become more widespread in recent years. However, their higher yield strength and rapid work-hardening behavior make springback more difficult to anticipate during panel and tooling design, and harder to control in tryout. Furthermore, for many parts with complex geometries the adjustment for springback based on personal experience is no longer adequate. In recent years, researchers and stamping engineers start to make die compensation by using computer simulations before cutting physical dies (Ref 1, 2) where springback analysis is carried out to obtain compensation directions and magnitudes before any necessary die compensation. Accordingly the accuracy of springback prediction becomes crucial to the success of any die compensation strategy whose algorithm relies on simulated springback.

Unfortunately accurate springback prediction still remains a formidable challenge despite tremendous efforts from both academic and industrial research. As we know, springback is due to the release of residual stresses accumulated during the forming stage. Accurate stress calculation is thus essential for obtaining the correct springback behavior. However, the stress calculations are less accurate than that of strain values calculated from currently available software. There are many factors affecting the stress accuracy in numerical simulations, including time integration schemes (implicit vs. explicit), element formulations, contact algorithms, and material models. In this paper, we focus our attention on the material modeling aspect with the aim to develop a more realistic and efficient constitutive relationship which is able to represent material deformation behavior more accurately.

Isotropic hardening is the simplest and most popular hardening model used today. It offers a reasonably good descriptions for monotonic loading cases and is relatively easy to implement in a finite element code. However, when materials experience unloading and then continue loading in the reverse direction, the model assumes that the material is hardened by the same amount in all directions and predicts that the material will only begin to yield when the effective stress level reaches the previously hardened level in the opposite direction. This is clearly in contradiction to experimental evidences known as Bauschinger effect. Figure 1 illustrates such phenomena where the yield stress in reverse loading is usually lower than that in the case of continued monotonic loading. On the other hand, a purely kinematic hardening model was first introduced by Prager and Ziegler where the yield surface translates in the stress space as material yields. However, this model ignores hardening effects in other stress directions.

Materials in general experience very complicated deformation during sheet metal forming process. Cyclic bending and unbending occur when the sheet passes through a drawbead or die radius. In order to represent the cyclic behavior more realistically, hardening rules combining both isotropic hardening and kinematic hardening were later developed by various researchers (Ref 3-6). Noticeably among them is a multi-yield

Danielle Zeng and **Z. Cedric Xia,** Scientific Research Laboratories, Ford Motor Company, Dearborn, MI 48121. Contact e-mail: zxia@ford.com.
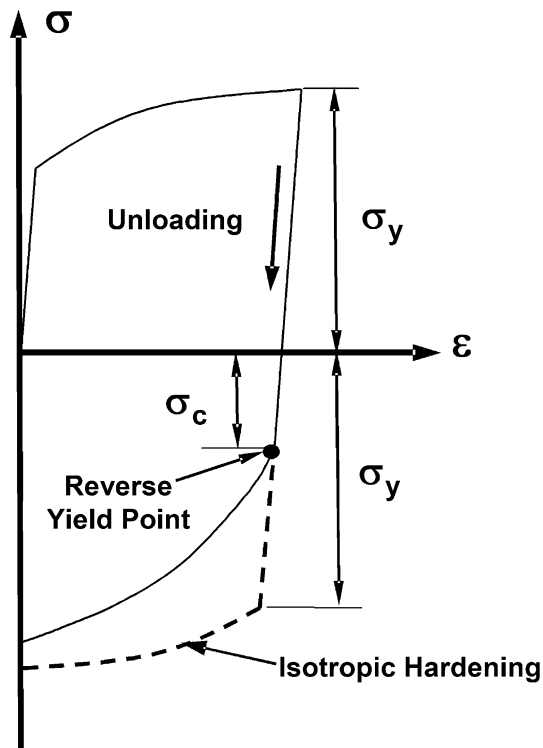
Fig. 1 Illustration of the Bauschinger effect. The dotted line shows material behavior under the isotropic hardening assumption. The material actually yields earlier if Bauschinger effect is present ($\sigma_c < \sigma_Y$)

Fig. 2 Illustration of multi-yield surfaces for isotropic materials

surface model proposed by Mroz (Ref 7, 8), which aims to describe the non-linear hardening behavior and the smooth transition from elastic to plastic deformation. This model introduces the concept of a field of work-hardening moduli to model the non-linear hardening behavior instead of a single modulus used in most of other kinematic models. Chu (Ref 9) generalized Mroz's discrete multiple yield surface concept into a continuous field of yield surfaces and Tang (Ref 10) and Tang et al. (Ref 11) used the model to analyze sheet metal formability and springback.

The Mroz model has several advantages over other more complex hardening models. It captures anisotropic hardening behavior nicely during reverse loading and it reduces to isotropic hardening for monotonic loading. One of its most appealing characteristics for sheet metal forming analysis and springback in particular is that the formulation does not require any additional experimental tests beyond standard uni-axial tensile curves. In fact there are no extra parameters required to fit the model, just the same as for isotropic hardening. However, the model also assumes that the material elastic unloading and reverse loading region is constant and twice the size of the initial yield stress. While this might be the case for single crystals and for some low-yield alloys, experimental evidence suggests that it is not the case in general for polycrystalline alloys, and Han et al. (Ref 12) found that the amount of Bauschinger effect actually depends on the hardening magnitude the material has experienced before the reverse loading.

The Mroz model as proposed originally in (Ref 7), described in (Ref 8), and extended in (Ref 9) assumes an isotropic Von Mises yield surface. However, it is well known that most of
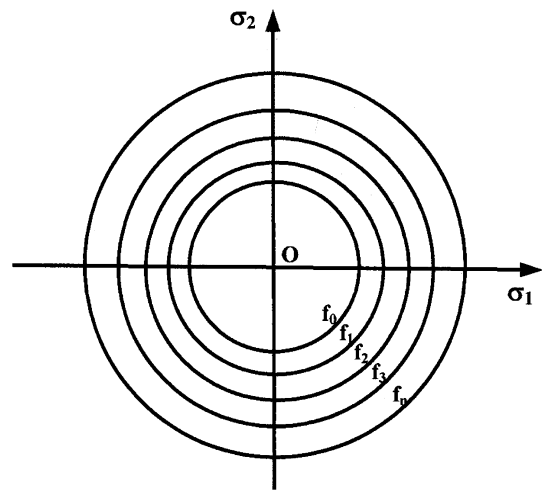
sheet metals exhibit strong directional dependence for both in-plane and normal-to-plane orientations. For such materials, Hill's anisotropic yield surface or other models developed recently tend to provide a better characterization of material's behavior. To this end, a modified Mroz model is proposed in this paper to take into account both the variable Bauschinger stresses and the anisotropic yield surface. Its constitutive integration algorithm is derived and implemented in FEA code for sheet metal forming analysis.

The paper is organized as follows: First, a brief review of the original Mroz model is outlined. The new model incorporating more accurate Bauschinger effect and anisotropic yielding is then proposed and discussed in detail, followed by the derivation of its constitutive integration algorithm and implementation in commercial FEA codes. The proposed model is applied to a simple test case for springback prediction. Experiments are conducted and results are compared with numerical prediction to demonstrate the new model's applicability.

2. Review of Mroz Multi-Surface Model

A brief review of the original Mroz model is presented here as the basis for later development. The general rule governing the evolution of multi-yield surfaces in Mroz model can be explained by considering the process of uni-axial loading, unloading and reverse loading of an initially isotropic material. As shown in Fig. 2 with a geometric interpretation of yield surfaces, the stress space is separated by a set of concentric surfaces into different regions and each region is associated with a hardening modulus. The innermost region, enclosed by f_0, is the elastic region, and the outermost surface f_n is the bounding surface.

As shown in Fig. 3(a), when a material point starts to load, beginning from zero stress state (point O) until reaching initial yielding (point A), all the circles remain fixed and are centered about O. In the figure, circle f_0 with solid line represents the active yield surface on which the current yield point is located. The circles with dotted line represent the inactive yield surfaces in the stress space.
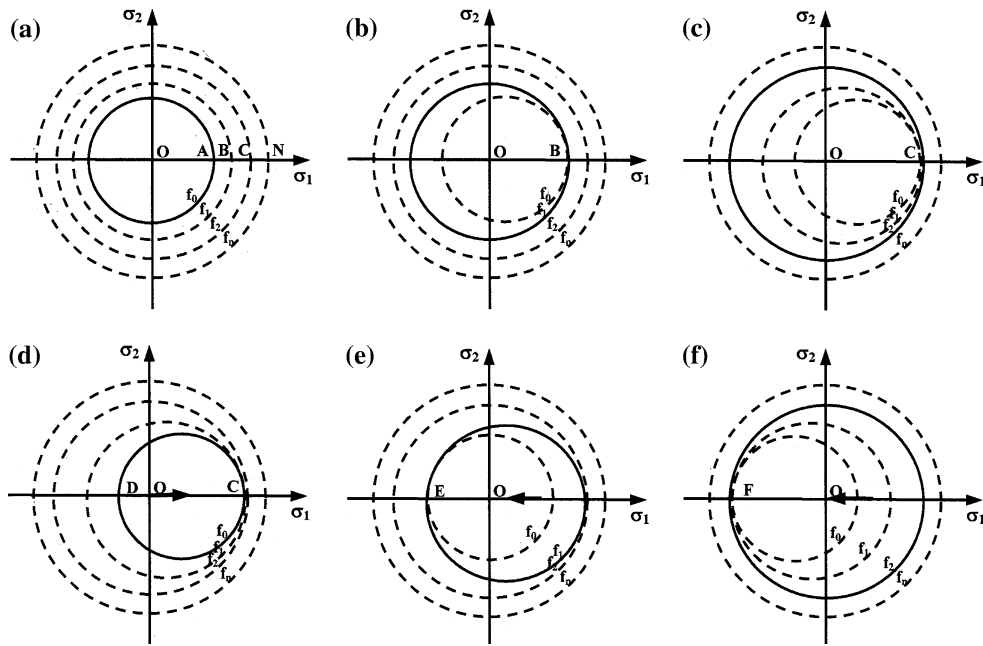
Fig. 3 Evolution of the multi-yield surfaces in the stress space under reverse loading

As a geometric interpretation, all yield circles are treated as rigid rings. To illustrate how the yield surface evolves upon loading, let us assume the material is stressed in the deviatric 1-direction (σ_1 only). When the specimen is loaded beyond elasticity, surface f_0 begins to move along σ_1 axis until it touches surface f_1 at point B (Fig. 3b). Circle f_1 then becomes active. During this process, other surfaces, except f_0, remain stationary. If the specimen is further loaded, f_0 and f_1 will move together along σ_1 axis while others remain still. This process will continue until f_0 and f_1 contact f_2 at point C (Fig. 3c). Surfaces f_0, f_1 and f_2 will then move together along the σ_1 axis if the load continues to increase. From Fig. 3(a)-(c), if we follow the path of the active surfaces and if the discretion of yield surfaces is made infinitely small, all the active yield surfaces will be continuous and centered at point O. Their expansion follows the same rule as that of isotropic hardening. There is no translation of the yield surface.

If the unloading process is initiated, all circles initially remain stationary during the elastic unloading phase, until the stress point moves from point C to D, as in Fig. 3(d), and f_0 again becomes the active yield surface. The arrow in Fig. 3(d) points to the moving direction of active yield surface center. When the reverse loading begins, f_0 will move along the σ_1 axis until point D reaches point E, as shown in Fig. 3(e). If the reverse loading continues, f_0 and f_1 will move together along σ_1 axis until point E reaches point F (shown in Fig. 3f).

Figure 4 shows the stress-strain curve of the uni-axial loading and unloading behavior described above. It follows the solid line OABCDEF as corresponding to the same points shown in Fig. 3. The dotted line corresponds to the modified Mroz model to be proposed later in this paper.

The model was further developed by Chu (Ref 9) where the discrete multiple yield surfaces were generalized into a continuous field of yield surfaces and is more suitable for FEA implementation. Interested readers should find detailed descriptions in (Ref 9).
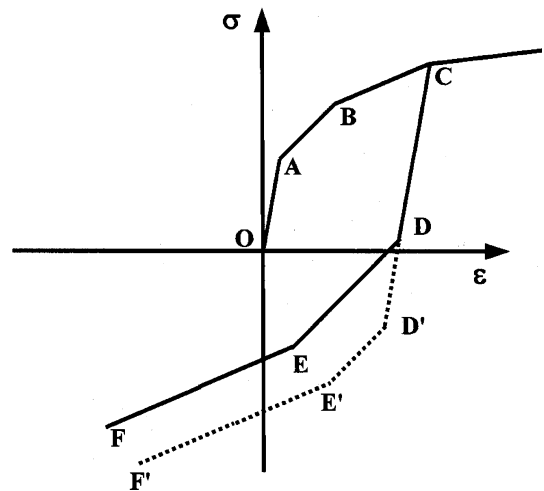

Fig. 4 Uni-axial stress-strain curves during reverse loading for Mroz model. The dotted line is for the modified Mroz model introduced in the current paper

3. Modified Mroz Model

The line CD in Fig. 4 represents the material elastic unloading behavior. The material begins to yield at the Point D during reverse loading after it unloads from Point C, and Point D represents the compressive yield strength according to the Mroz model. This model assumes that the size of elastic region is constant as characterized by the initial yield stress. The elastic range during reverse loading equals twice that of the initial yield strength. Thus when the material hardens and then unloads, lower compressive yield strength than the initial yield is obtained. The lower solid line in Fig. 5 is the reversal of compressive yield strength curve at the corresponding reverse point according to Mroz model for a typical DP600 steel. It

shows that in the model as the tensile strength increases, the corresponding compression strength decreases. For the material with higher work hardening, it is conceivable that the reverse yield point will go to zero or even become positive (in tension), i.e., the model predicts that the material might enter reverse plastic loading while it is released from uni-axial tension even if there is no external forces applied. This is contradictory to what was observed in real material compression testing (Ref 12). Figure 6 shows the compressive yield strength at various tensile reversal points obtained from compression testing for different grades of steels. The data suggests that when the load reverses at higher strength point, the compressive yield strength is higher or at least in the same level. According to the test data, the compressive yield strength curve should follow the dotted pink line instead of the solid line in Fig. 5 as predicted by Mroz model. Clearly the Mroz model as it is now cannot adequately represent material deformation behavior under reverse loading.

Towards the end we propose a modified Mroz model to address its drawbacks as discussed above while preserving its original formulation. In this modification, the material deformation follows the same rule as that of Mroz model at monotonic loading. However, when the unloading is initiated, the size of the innermost yield surface (for elastic deformation) is no longer prescribed as the size of the initial yield surface. Rather it is determined through a reverse compression test. Therefore, instead of line CD in Fig. 4, the elastic unloading
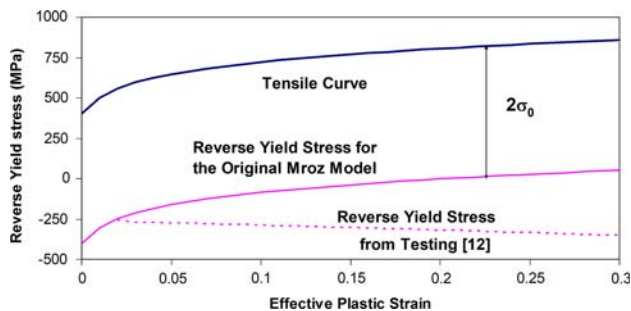

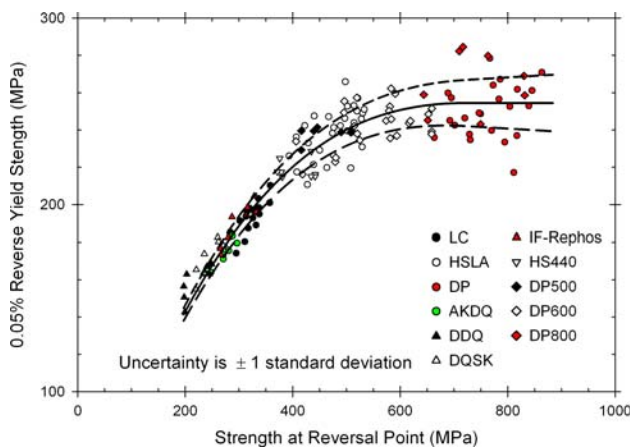**Fig. 5** Reverse yield stress as a function of the effective plastic strain

Fig. 6 Yield strength (0.05% offset) on reversal as a function of steel strengths before reverse loading (from (12))

curve becomes CD′, where D′ is the compressive yield strength at the reverse point C obtained from the standard compression testing. Based on this modification, the size of the elastic region σ_B is a function of equivalent plastic strain ε^{pl} and can be expressed as:

$$\sigma_B = \frac{1}{2}\left(\sigma_Y + |\sigma_c|\right) \tag{Eq 1}$$

where σ_Y is the current flow stress and σ_c is the compressive yield stress at corresponding reversal point from reverse compression testing. σ_B can be rewritten in the following generalized form:

$$\sigma_B = c\sigma_0 + (1-c)\sigma_Y \tag{Eq 2}$$

where σ_0 is the initial yield stress of the material, and c is a material parameter reflecting the Bauschinger effect and is considered to be a function of the effective plastic strain. It is easy to note that isotropic hardening is a special case of this model when $c \equiv 0$ (thus $\sigma_B = \sigma_Y$), and the model is reduced to the original Mroz model when c is taken to be 1 ($c \equiv 1$, with $\sigma_B = \sigma_0$). In its most general form, c is a function of ε^{pl}, where it can be expressed as:

$$c(\varepsilon^{pl}) = \begin{cases} \frac{1}{2}\frac{\sigma_y - |\sigma_c|}{\sigma_y - \sigma_0} & \text{when } \sigma_y > \sigma_0 \\ 0 & \text{when } \sigma_y = \sigma_0 \end{cases} \tag{Eq 3}$$

It should be noted that the value of c does not matter if $\sigma_y = \sigma_0$, and we always have $\sigma_B \equiv \sigma_0$.

4. Formulation and Constitutive Integration of the Modified Mroz Model

The material constitutive relationship and its integration for numerical implementation will be derived in this section. Since most sheet metals exhibit different yield strengths along different directions, Hill's anisotropic yield criterion is used in this paper to characterize the material anisotropic behavior. For the case of combined isotropic-kinematic hardening, the plastic yield criterion can be expressed as,

$$f(\boldsymbol{\sigma}) \equiv \sqrt{\frac{3}{2}(\boldsymbol{\sigma}-\boldsymbol{\alpha})^T P (\boldsymbol{\sigma}-\boldsymbol{\alpha})} - Y(\varepsilon^{pl}) \tag{Eq 4}$$

where $\boldsymbol{\sigma} = \{\sigma_{11}, \sigma_{22}, \sigma_{33}, \sigma_{12}, \sigma_{23}, \sigma_{13}\}^T$ is the stress vector in general 3D stress state, $\boldsymbol{\alpha} = \{\alpha_{11}, \alpha_{22}, \alpha_{33}, \alpha_{12}, \alpha_{23}, \alpha_{13}\}^T$ are stress values representing the center of currently active yield surface, $Y(\varepsilon^{pl})$ is the material flow stress and is generally a function of equivalent plastic strain ε^{pl}, and P is a 6×6 anisotropic plasticity matrix in general 3D case and can be expressed in terms of the anisotropic r-values in three orientations as:

$$P = \frac{2}{3}\begin{bmatrix} 1 & -\frac{r_0}{r_0+1} & -\frac{1}{r_0+1} & 0 & 0 & 0 \\ -\frac{r_0}{r_0+1} & \frac{r_0(r_{90}+1)}{r_{90}(r_0+1)} & -\frac{r_0}{r_{90}(r_0+1)} & 0 & 0 & 0 \\ -\frac{1}{r_0+1} & -\frac{r_0}{r_{90}(r_0+1)} & \frac{r_0+r_{90}}{r_{90}(r_0+1)} & 0 & 0 & 0 \\ 0 & 0 & 0 & \frac{(2r_{45}+1)(r_0+r_{90})}{r_{90}(r_0+1)} & 0 & 0 \\ 0 & 0 & 0 & 0 & 3 & 0 \\ 0 & 0 & 0 & 0 & 0 & 3 \end{bmatrix}$$
$$\tag{Eq 5}$$

According to Hooke's law, the stress vector can be obtained through elastic strain as:

$$\boldsymbol{\sigma}_{t+\Delta t} = \mathbf{D}\boldsymbol{\varepsilon}_{t+\Delta t}^{\mathrm{el}} \qquad \text{(Eq 6)}$$

where $\mathbf{D}$ is a 6×6 elastic modulus matrix. According to incremental plastic flow theory, all the variables at time step $t + \Delta t$ can be calculated once the deformation history at last time step t is known. Thus the elastic strain $\boldsymbol{\varepsilon}_{t+\Delta t}^{\mathrm{el}}$ can be expressed as:

$$\boldsymbol{\varepsilon}_{t+\Delta t}^{\mathrm{el}} = \boldsymbol{\varepsilon}_t^{\mathrm{el}} + d\boldsymbol{\varepsilon} - d\boldsymbol{\varepsilon}^{\mathrm{pl}} \qquad \text{(Eq 7)}$$

Here $\boldsymbol{\varepsilon}_t^{\mathrm{el}}$ is the elastic strain at time t, $d\boldsymbol{\varepsilon}$ and $d\boldsymbol{\varepsilon}^{\mathrm{pl}}$ are the total strain increment and plastic strain increment vectors, respectively. The associated flow rule gives:

$$d\boldsymbol{\varepsilon}^{\mathrm{pl}} = \Delta\varepsilon^{\mathrm{pl}} \frac{\partial f}{\partial \boldsymbol{\sigma}}\Big|_{t+\Delta t} \qquad \text{(Eq 8)}$$

where $\Delta\varepsilon^{\mathrm{pl}}$ is the equivalent plastic strain increment. Also, during the plastic loading,

$$f(\boldsymbol{\sigma}) \equiv 0 \qquad \text{(Eq 9)}$$

Thus, from Eqs. (4) and (9), we have

$$\frac{\partial f}{\partial \boldsymbol{\sigma}}\Big|_{t+\Delta t} = \frac{3}{2Y}\mathbf{P}(\boldsymbol{\sigma}_{t+\Delta t} - \boldsymbol{\alpha}_{t+\Delta t}) \qquad \text{(Eq 10)}$$

Therefore

$$d\boldsymbol{\varepsilon}^{\mathrm{pl}} = \frac{3\Delta\varepsilon^{\mathrm{pl}}}{2Y}\mathbf{P}(\boldsymbol{\sigma}_{t+\Delta t} - \boldsymbol{\alpha}_{t+\Delta t}) \qquad \text{(Eq 11)}$$

Substituting Eqs. (7) and (11) into Eq. (6), we get:

$$\boldsymbol{\sigma}_{t+\Delta t} = \boldsymbol{\sigma}^* - \frac{3\Delta\varepsilon^{\mathrm{pl}}}{2Y}\mathbf{D}\mathbf{P}(\boldsymbol{\sigma}_{t+\Delta t} - \boldsymbol{\alpha}_{t+\Delta t}) \qquad \text{(Eq 12)}$$

where $\boldsymbol{\sigma}^*$ is usually termed as stress predictor:

$$\boldsymbol{\sigma}^* = \mathbf{D}(\boldsymbol{\varepsilon}_t^{\mathrm{el}} + d\boldsymbol{\varepsilon}) \qquad \text{(Eq 13)}$$

The stress vector can be re-written as:

$$\boldsymbol{\sigma}_{t+\Delta t} - \boldsymbol{\alpha}_{t+\Delta t} = \mathbf{M}(\boldsymbol{\sigma}^* - \boldsymbol{\alpha}_{t+\Delta t}) \qquad \text{(Eq 14)}$$

where

$$\mathbf{M} = \left[\mathbf{I} + \frac{3\Delta\varepsilon^{\mathrm{pl}}}{2Y}\mathbf{D}\mathbf{P}\right]^{-1} \qquad \text{(Eq 15)}$$

The position of active yield surface center $\boldsymbol{\alpha}$ at time $t + \Delta t$ can be determined according to the rule of Mroz model. As shown in Fig. 7, F_t is the active yield surface with center O at time t. F_I is the inactive yield surface with center O_I in memory and tangent to surface F_t at point P. $F_{t+\Delta t}$ is the active yield surface with center O′ at next time step $t + \Delta t$. $\boldsymbol{\beta}$ is a unit vector representing the moving direction of the center of current yield surface and can be expressed as:

$$\boldsymbol{\beta} = \frac{\boldsymbol{\alpha}_I - \boldsymbol{\alpha}_t}{\sqrt{\frac{3}{2}(\boldsymbol{\alpha}_I - \boldsymbol{\alpha}_t)^{\mathrm{T}}\mathbf{P}(\boldsymbol{\alpha}_I - \boldsymbol{\alpha}_t)}} \qquad \text{(Eq 16)}$$

Then the amount of active yield surface center movement from time t to $t + \Delta t$ can be expressed as:

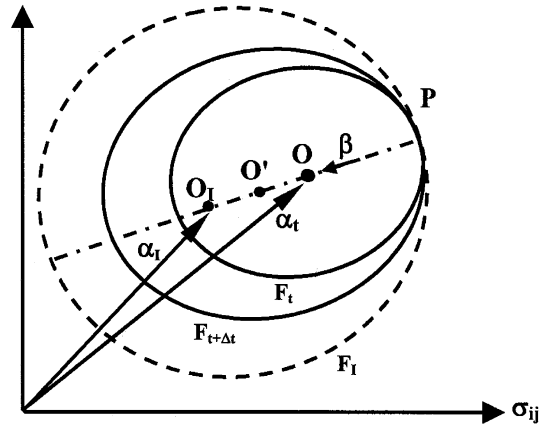$$d\boldsymbol{\alpha} = dY\boldsymbol{\beta} \qquad \text{(Eq 17)}$$

Fig. 7 Illustration of the active yield surface movement

where dY is the increment of the active yield surface radius from time t to $t + \Delta t$ and is a function of $\Delta\varepsilon^{\mathrm{pl}}$. Substituting Eq. (14) into (9) and together with (4), Eq. (9) becomes

$$f(\Delta\varepsilon^{\mathrm{pl}}) = \sqrt{\frac{3}{2}[\mathbf{M}(\boldsymbol{\sigma}^* - \boldsymbol{\alpha}_{t+\Delta t})]^{\mathrm{T}}\mathbf{P}[\mathbf{M}(\boldsymbol{\sigma}^* - \boldsymbol{\alpha}_{t+\Delta t})]} - Y(\varepsilon^{\mathrm{pl}}) = 0 \qquad \text{(Eq 18)}$$

$\Delta\varepsilon^{\mathrm{pl}}$ is the only unknown in this non-linear equation and can be solved numerically with methods such as the Newton-Raphson algorithm outlined in (Ref 13).

It is also necessary to obtain material stiffness matrix $(d\boldsymbol{\sigma}/d\boldsymbol{\varepsilon})$ if implicit time integration FEA is adopted. It can be expressed as, after some algebra from taking the derivative of Eq. (12):

$$\frac{d\boldsymbol{\sigma}}{d\boldsymbol{\varepsilon}} = \left\{\mathbf{D}^{-1} + \frac{(\partial f/\partial \boldsymbol{\sigma})(\partial f/\partial \boldsymbol{\sigma}^{\mathrm{T}})}{Y'\left(1 + \frac{\partial f}{\partial \boldsymbol{\sigma}^{\mathrm{T}}}\boldsymbol{\beta}\right)}\right\}^{-1} \qquad \text{(Eq 19)}$$

where $Y' = dY(\varepsilon^{\mathrm{pl}})/\varepsilon^{\mathrm{pl}}$.

5. Experimental and Numerical Example

5.1 Experiment

Based on the formulation derived above, a material user-subroutine was developed to compute the elastic-plastic constitutive equation, and has been implemented in the implicit commercial software ABAQUS/Standard. The user subroutine can be used for 3D solid, plane stress shell, 2D plane stress and plane strain elements.

A straight U-channel draw test was conducted to test the ability of the proposed model in predicting the springback. Figure 8 shows the geometry of the tooling set up. The upper die radius is 12 mm and the lower die radius is 6 mm. The punch width is 50 mm with a 2.5 mm radius. The radius of the drawbead is 6 mm.

A variety of tests were conducted with different materials, blank holder forces, and with and without drawbeads. The case presented in this paper is a 1.5 mm DP600 blank with drawbead and blank holder force of 100 kN. The blank size

is 240×100 mm^2. The draw depth is 70 mm and it runs through the width of the blank (100 mm). Figure 9 shows the picture of testing piece in this loading case after springback. It is observed that the DP600 part has much larger springback than mild steel parts, both in the wall open (as defined by the angle of the flange from the horizontal surface) and side wall curl.

The material properties of DP600 are listed in Table 1. Figure 10 is its stress-plastic strain curve obtained from uni-axial tensile test. In the physical testing, the blank was wrapped
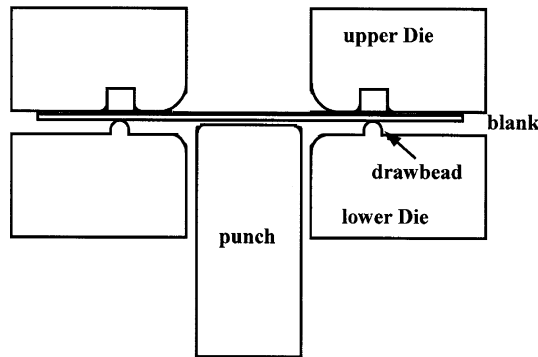

Fig. 8 Experimental set up of the U-channel test

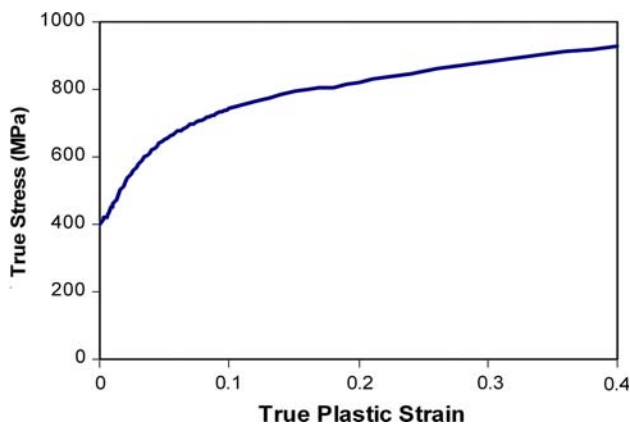**Fig. 9** A picture of the formed DP600 U-channel showing springback

Fig. 10 Stress-plastic strain curve for the DP600 steel in the U-channel test

by a teflon sheet to reduce the friction. In the numerical simulation, a frictional coefficient of 0.08 is used in the Coulomb friction model.

5.2 Effect of Anisotropic Yield Surface

The effect of anisotropic yield criterion on the springback prediction was investigated numerically. Finite element simulations were conducted in ABAQUS for the U-channel tests. Only half of the U-channel was modeled because of the symmetry. Four-node plane strain elements were employed with eight layers through thickness and the in-plane element size is about 0.5 mm. Simulations with even finer meshes were performed and did not have any appreciable differences in results. Figure 11 consists of three numerical simulation results with different yield surface characterizations and numerical implementations as well as experimental result. For all three simulation results the isotropic hardening flow rule was used. This was achieved in the modified Mroz model by setting $c = 0$ in Eq. (2). Hill's anisotropic yield function was used in both the modified Mroz model and ABAQUS own constitutive model with isotropic hardening. These two are equivalent and therefore should yield exactly the same simulation results. They were therefore used to verify numerical implementation of the user-material subroutine.

Their numerical results indeed matched as shown in Fig. 11. In addition, the springback prediction by ABAQUS standard with the isotropic yield function was also obtained and plotted

Table 1 DP600 steel material properties

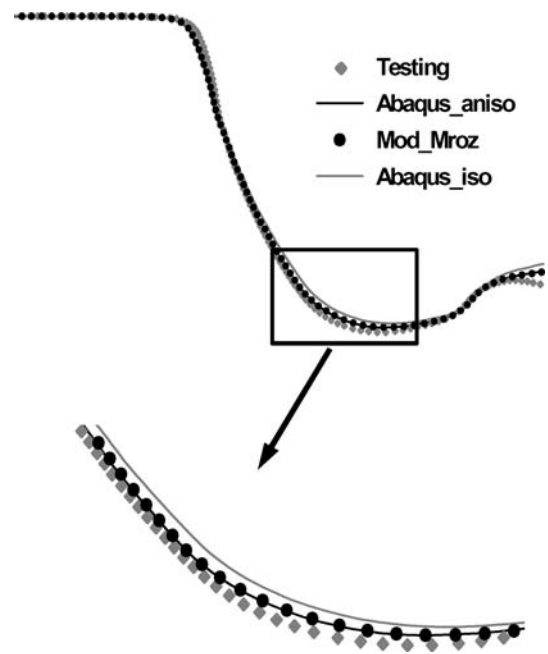| Material	E	ν	r_0	r_{45}	r_{90}	σ_0
DP600	221 GPa	0.3	0.54	0.88	0.99	402 MPa

Fig. 11 Springback results from the experiment and from simulations with different yield surface (all three models assume isotropic hardening)
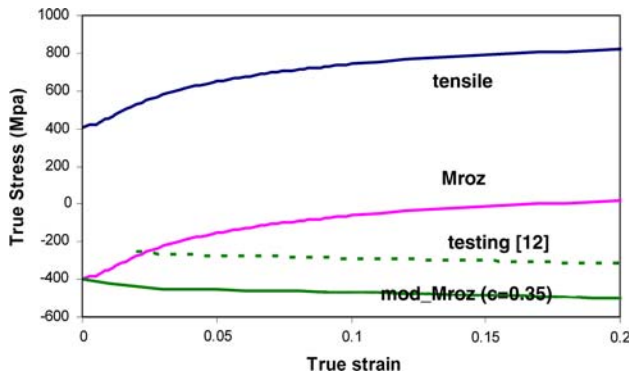
Fig. 12 Compressive yield strength on reversal as a function of true strain before unloading
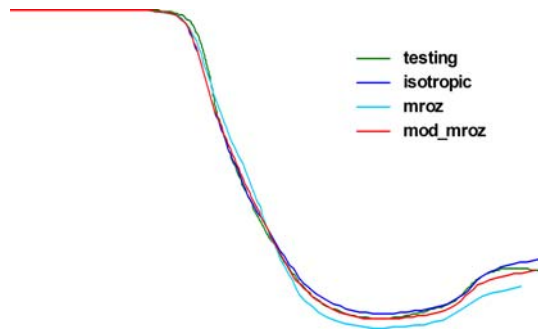

Fig. 13 Comparison of springback results for three material hardening models

together in Fig. 11. It can be seen that the predictions with anisotropic yield function (by either the Modified Mroz model with $c = 0$ or ABAQUS own anisotropic yield model) gave a better prediction of the springback as compared with the testing result than that of using an isotropic yield function. It is thus important to include material anisotropy in numerical simulations.

5.3 Numerical Result for the Modified Mroz Model

In addition to the standard stress-strain curve under uni-axial tension, the Modified Mroz model requires the compression yield stress at corresponding reversal points as its input (Eq. 3). Since the available compression data are very limited in the literature, the compressive yield stress adopted in the current study is obtained by offsetting the testing reverse yield curve from (Ref 12) (shown in Fig. 12) down to the point that compression yield stress is same as the tensile yield stress at zero strain reverse point. The reason that the offset is necessary is due to the fact that the yield stress was obtained by a 0.05% offset in (Ref 12), not the standard 0.2% offset for yield strength measurement. The resulting c value in Eq. (2) is about 0.35 as shown in Fig. 12.

Numerical results for predicted springback are shown in Fig. 13 for three material models as well as the test result. They are the isotropic hardening model, the original Mroz model, and the Modified Mroz model introduced in this study. The anisotropic yield was accounted for in all three material models. The test results were measured by a CMM scan at the outer surface of the specimen. Three repeats were conducted

under the same conditions and the variations of measurements were small from specimen to specimen and from the left half to the right half. The test result presented in Fig. 13 was taken from one side of the one set of the data. It is evident from Fig. 13 that the prediction of Mroz model gives largest deviation from testing data while that of modified Mroz model goes between the isotropic hardening model and Mroz model, and it is closest to the testing result. This indicates that the Bauschinger effect is actually not as big as assumed by the original Mroz model, and is best characterized by the modified Mroz model.

6. Discussions

A modified Mroz model is introduced in this paper to predict the springback for sheet metal forming and springback prediction, and is believed to be especially advantageous for AHSS. The model combines the material isotropic hardening and kinematic hardening, and also considered the anisotropic yield criterion. The material reverse loading behavior is incorporated in the model to adequately represent actual Bauschinger effect under cyclic loading. The springback prediction by the proposed model for the DP600 U-channel correlates very well with experimental test. However, it should be cautioned that more reverse compression test data are needed to enable wide applications of this model, and an extensive study for more complex forming operations is necessary to demonstrate its effectiveness in springback prediction.

References

1. L. Wu, Tooling Mesh Generation Technique for Iterative FEM Die Surface Design Algorithm to Compensate for Springback in Sheet Metal Stamping, *Eng. Comput.*, 1997, **14**(6), p 630–648
2. L. Geng, T. Oetjens, and C.-Y. Sa, Springback Prediction with LS-DYNA and Die Face Compensation of Aluminum Hood Inner, SAE2003-01-0571
3. J.L. Chaboche, Time-Independent Constitutive Theories for Cyclic Plasticity, *Int. J. Plasticity*, 1986, **2**(2), p 149–188
4. B.K. Chun, J.T. Jinn, and J.K. Lee, Modeling the Bauschinger Effect for Sheet Metals, part I: Theory, *Int. J. Plasticity*, 2002, **18**, p 571–595
5. K. Chung, M. Lee, D. Kim, C. Kim, M.L. Wenner, and F. Barlat, Spring-Back Evaluation of Automotive Sheets Based on Isotropic-Kinematic Hardening Laws and Non-Quadratic Anisotropic Yield Functions, Part I: Theory and Formulation, *Int. J. Plasticity*, 2005, **21**, p 861–882
6. L. Geng, Y. Shen, and R.H. Wagoner, Anisotropic Hardening Equations Derived from Reverse-Bend Testing, *Int. J. Plasticity*, 2002, **18**, p 743–767
7. Z. Mroz, On the Description of Anisotropic Work Hardening, *J. Mech. Phys. Solids*, 1967, **15**, p 163–175

8. A.S. Khan and S. Huang, *Continuum Theory of Plasticity*, Wiley-Interscience Publication, 1995

9. C.C. Chu, A Three-Dimensional Model of Anisotropic Hardening in Metals and its Application to the Analysis of Sheet Metal Formability, *J. Mech. Phys. Solids*, 1984, **32**(3), p 197–212

10. S.C. Tang, An Anisotropic Hardening Rule for the Analysis of Sheet Metal forming Operations, *Adv. Technol. Plasticity*, 1990, **3**, p 1149–1154

11. S.C. Tang, Z.C. Xia, and F. Ren, Application of the Radial Return Method to Compute Stress Increments from Mroz's Hardening Rule, *J. Eng. Mater. Tech.*, 2001, **123**, p 398–402

12. K. Han, C.J. Van Tyne, and B.S. Levy, Bauschinger Effect Response of Automotive Sheet Steel, SAE 2005-01-0084

13. W.H. Press, B.P. Flannery, S.A. Teukolsky, and W.T. Vetterling, *Numerical Recipes: The Art of Scientific Computing*, Cambridge University Press, 1986